THE GEOLOGICAL SOCIETY OF AMERICA®

Differential compaction over Late Miocene submarine channels in SE Brazil: Implications for trap formation

Nicholas I.P. Ward†, Tiago M. Alves, and Tom G. Blenkinsop
3D Seismic Laboratory, School of Earth and Ocean Sciences, Cardiff University, Main Building Park Place, Cardiff, CF10 3AT, UK

ABSTRACT

We used high-quality three-dimensional (3-D) seismic data to quantify the timing and magnitude of differential compaction over a Late Miocene submarine channel complex in SE Brazil (Espírito Santo Basin). A thickness-relief method was applied to quantify the thickness variations in strata deposited over the channel complex. We found that differential compaction started after the channel complex was buried by ~200 m of strata, as revealed by thinning horizons observed over a compaction-related anticline. The size of the anticline is greatest in the south of the study area, reaching heights of 41 ms (~50 m). Fluid expelled through faults on the margins of the channel complex formed large depressions. These depressions increased in size after deep-water currents removed the fluid-rich sediment filling them. Differential compaction also occurred over deposits downslope of knickpoints, reaching maximum heights of 29 ms (~35 m). Seismic reflections onlap the knickpoint face and are believed to comprise slumped strata and debrites. Two-way traveltime isochron and amplitude maps indicate that there are limited connectivity and lateral continuity of the coarse-grained units. Differential compaction over these deposits created anticlines with four-way dip closure. As a consequence, isolated reservoirs were closed vertically by the compaction anticlines and laterally by strata onlapping the knickpoint face. These unique reservoirs could have been charged by migration of hydrocarbons along sands at the base of the channel complex. A fill-to-spill model is hypothesized using the above mechanism: Once an isolated anticlinal trap reached spill point, hydrocarbons migrated upslope into the next trap. Traps like these could form above submarine channels in similar basins around the world (e.g., Gulf of Mexico, west coast of Africa) after early burial.

†wardni@cardiff.ac.uk

INTRODUCTION

Compaction of sediments during the early stages of burial is closely related to lithology and water content (Athy, 1930; Trask, 1931). All porous sediments tend to compact under increasing burial depth, with the greatest amount of compaction occurring in intervals with the highest porosity (Perrier and Quiblier, 1974). Consequently, clays and shales compact more than sandstones and conglomerates, a phenomenon leading to differential compaction (Chopra and Marfurt, 2012; Clark and Pickering, 1996; Cosgrove and Hillier, 1999; Perrier and Quiblier, 1974; Posamentier, 2003; Trask, 1931). Structures associated with differential compaction commonly include anticlines over the less compacted lithology (Alves, 2010; Chopra and Marfurt, 2012; Cosgrove and Hillier, 1999; Heritier et al., 1980; Posamentier, 2003). This study examined compaction-related anticlines over a submarine channel complex, particularly those formed over coarse-grained sediment bodies deposited downstream of knickpoints, where marked increases in the gradient of the channel complex were observed (Heiniö and Davies, 2007; Howard et al., 1994).

Positive relief structures that are concomitant with differential compaction over sandy intervals form very effective hydrocarbon traps. Many producing fields around the world present these types of features, particularly in the North Sea (Corcoran, 2006; Cosgrove and Hillier, 1999; Heritier et al., 1980), Canada (Wood and Hopkins, 1989, 1992), and SE Brazil (Davison, 1999). Coarse-grained strata with high reservoir potential and low compaction rates are usually bounded laterally and vertically by less permeable, fine-grained sediment. This forms an effective seal for hydrocarbon reservoirs, which become stratigraphically and structurally trapped after compaction (Corcoran, 2006). However, a key problem faced when drilling compaction-related structures is the local development of overpressure in porous intervals. When compaction does not keep pace with sedimentation rate, fluids preferentially migrate toward permeable sands, creating local overpressure conditions (Osborne and Swarbrick, 1997). If pore pressure in the sand increases above the lithostatic pressure, the overburden fractures, allowing fluids to escape from potential reservoir intervals and migrate toward the surface (Davies, 2003; Gay et al., 2003).

Previous studies have focused on the seismic expression of differential compaction structures, their potential for forming hydrocarbon traps, and the causes for overpressure and fluid expulsion (Chopra and Marfurt, 2012; Corcoran, 2006; Cosgrove and Hillier, 1999; Gay et al., 2006a; Xu et al., 2015). Most of these studies have provided qualitative data on large, discrete structures. This study used a three-dimensional (3-D) seismic data set from Espírito Santo Basin, SE Brazil, to quantify the magnitude and timing of differential compaction over a submarine channel complex, and over strata deposited downslope of knickpoints (Fig. 1). A thickness-relief method, modified by Alves and Cartwright (2010) from Perrier and Quiblier (1974), was used to quantify the topographic expression of compaction-related anticlines and assess when differential compaction was initiated. The findings were supported with variance, amplitude, and thickness maps. This paper thus attempted to answer three key research questions:

(1) What is the magnitude and timing of differential compaction over channel-fill deposits?

(2) What are the main factors controlling differential compaction over the channel complex and knickpoints?

(3) What effect does differential compaction have on trap formation?

GEOLOGICAL SETTING

The Espírito Santo Basin is one of a number of Mesozoic rift basins offshore southeast Brazil (Fig. 1A). It is bounded by the Abrolhos Plateau to the north, and the Campos and Santos Basins to the south. These basins formed during the Late Jurassic to Cretaceous breakup of Gondwana as the South Atlantic began to open (Alves et al., 2009; Davison, 1999; Fiduk et al., 2004;

GSA Bulletin; January/February 2018; v. 130; no. 1/2; p. 208–221; https://doi.org/10.1130/B31659.1; 12 figures; published online 14 September 2017.

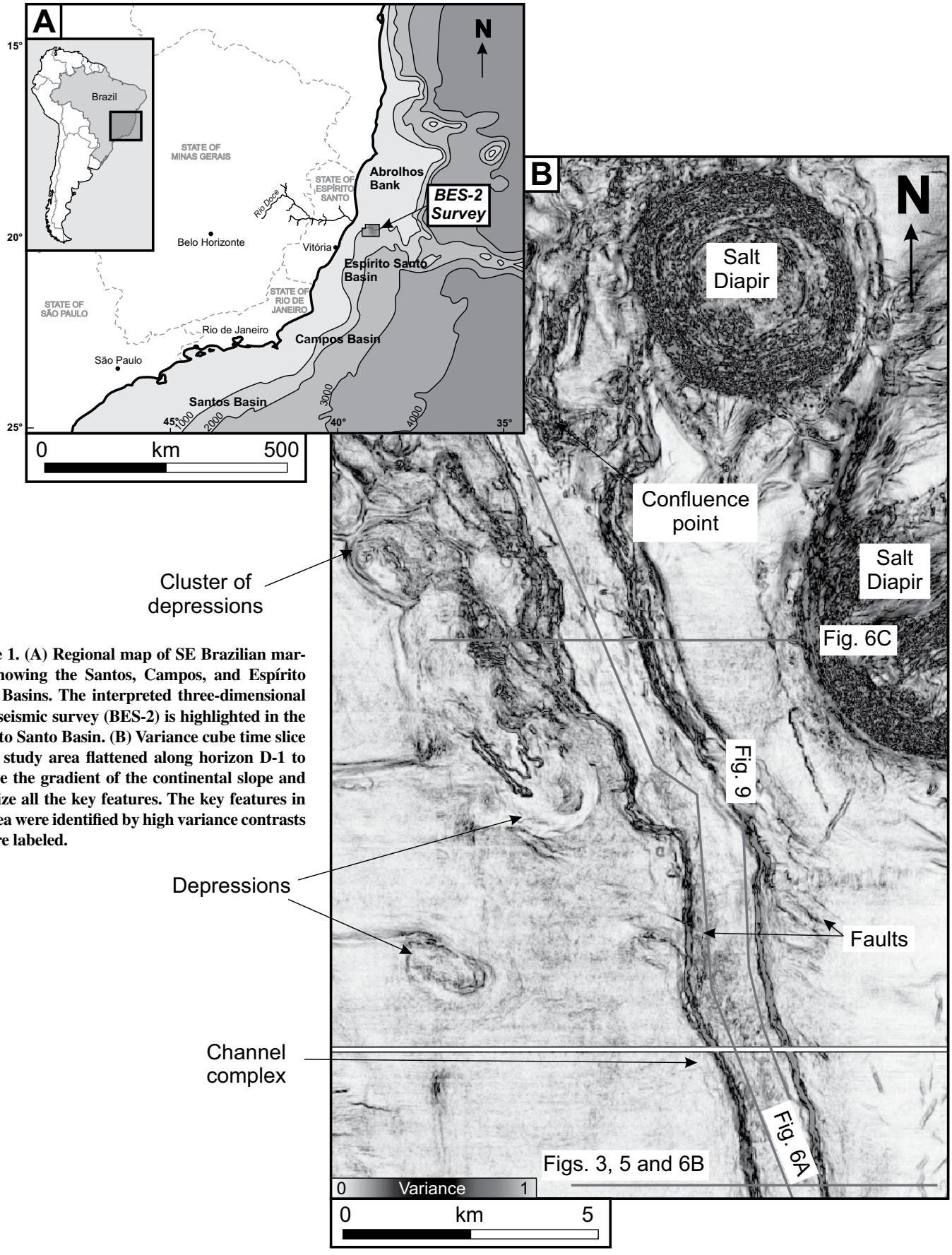

Figure 1. (A) Regional map of SE Brazilian margin, showing the Santos, Campos, and Espírito Santo Basins. The interpreted three-dimensional (3-D) seismic survey (BES-2) is highlighted in the Espírito Santo Basin. (B) Variance cube time slice of the study area flattened along horizon D-1 to remove the gradient of the continental slope and visualize all the key features. The key features in the area were identified by high variance contrasts and are labeled.

Gamboa et al., 2011). The study area is located on the southern bank of the Abrolhos Plateau, where submarine channels cut through Cenozoic strata on a southward-dipping continental slope (Fig. 1).

Three phases of basin evolution are recognized offshore Espírito Santo (Fig. 2). These are the synrift phase, postrift (transitional) phase, and the drift phase (Ojeda, 1982; Fig. 2). During the synrift phase (late Berriasian to early Aptian), continental sandstones, silts, and shales were deposited together with syntectonic conglomerates (Baudon and Cartwright, 2008; Chang et al., 1992; Gamboa et al., 2010; Ojeda, 1982). Deposition of coarse-clastic material alternated in space with basaltic volcaniclastic rocks (Chang et al., 1992). Stable tectonic conditions prevailed during the early to late Aptian, when postrift sediments were deposited (Baudon and Cartwright, 2008; Demercian et al., 1993; Ojeda, 1982). Two stages of evaporite deposits are recorded in this megasequence, clastic and carbonate deposition, separated by an unconformity. Thick salt units were deposited during the late Aptian in the Espírito Santo Basin (Gamboa et al., 2010; Mohriak et al., 2008).

The final drift phase occurred in two depositional megasequences: early and late drift (Fig. 3). The early drift stage is represented by two marine-transgressive sequences, with a shallow-water carbonate platform developing from the late Albian to Cenomanian. This platform is overlain by shales of Turonian to Paleocene age, indicating deepening of the basin (Demercian et al., 1993; Gamboa et al., 2010, 2011; Ojeda, 1982). A mid-Eocene sequence boundary occurs across the entire southeast Brazilian margin and separates the early drift stage from the late drift stage (Gamboa et al., 2011). Above this boundary, Eocene to Holocene siliciclastic sediments were deposited during a regressive period associated with sediment progradation on the continental slope (Chang et al., 1992; Demercian et al., 1993). Clastic sediments filling the basin at the time were derived from erosion of coastal mountain ranges and volcanic activity on the Abrolhos Plateau; the mountain uplift and erosion caused a regional mid-Eocene unconformity (Chang et al., 1992; Gamboa et al., 2010). Tuffs, volcanic breccias, and hyaloclastites represent the bulk of the volcaniclastic input, whereas fine to coarse massive sandstones, conglomerates, and siltstones were eroded from mountains (Gamboa et al., 2010).

Structural deformation in the Espírito Santo Basin was largely controlled by thin-skinned gravitational gliding over Aptian evaporites (Demercian et al., 1993; Fiduk et al., 2004). This process occurred throughout the Cenozoic, peaking during the Eocene–early Oligocene, and

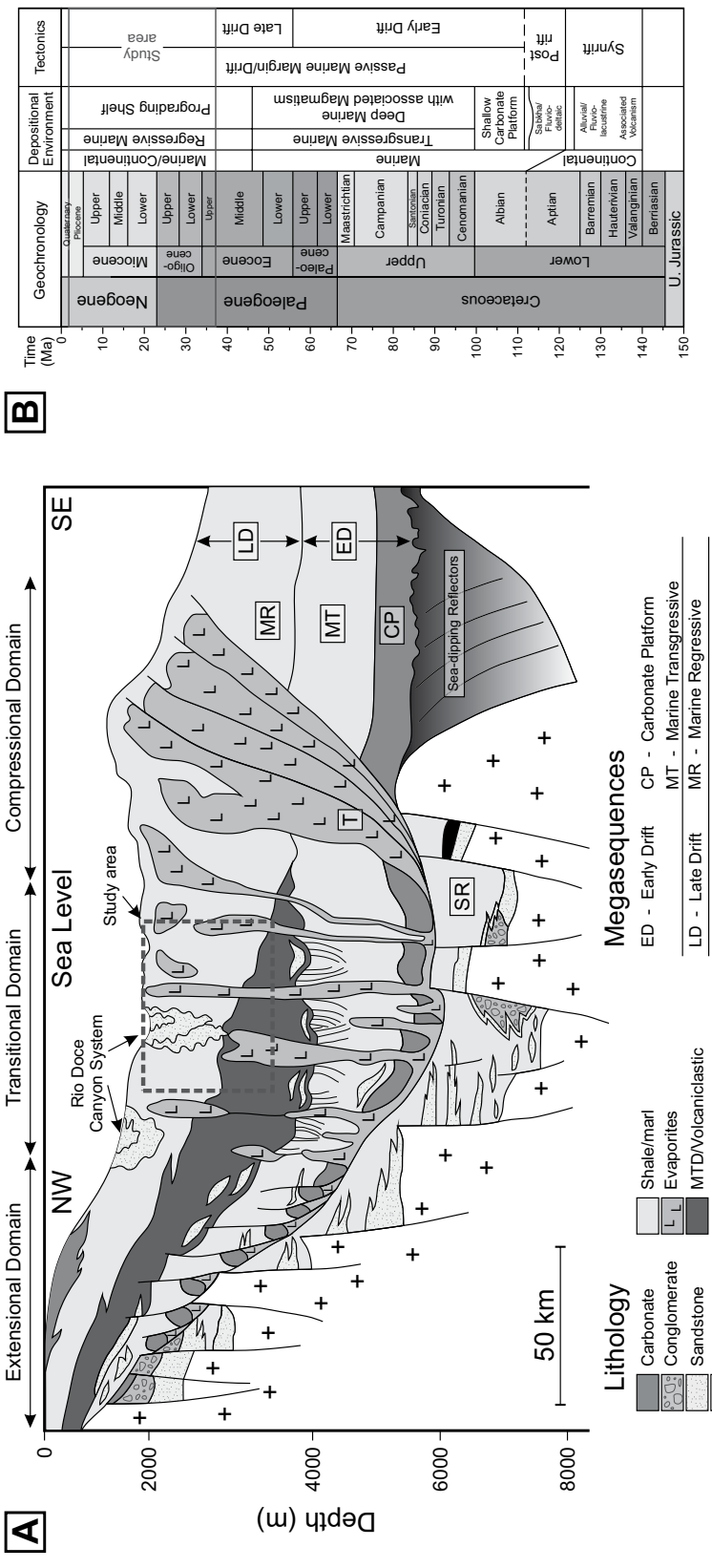

Figure 2. (A) Schematic diagram showing the megasequences in the Espírito Santo Basin. It also shows the structural domains developed within the basin. The study area lies within the transitional domain, and it focuses on the late drift sequence. MTD—mass-transport deposit. (B) Stratigraphic column showing the main depositional environments and timings of the megasequences in the Espírito Santo Basin, modified after Fiduk et al. (2004) and Gamboa et al. (2010).

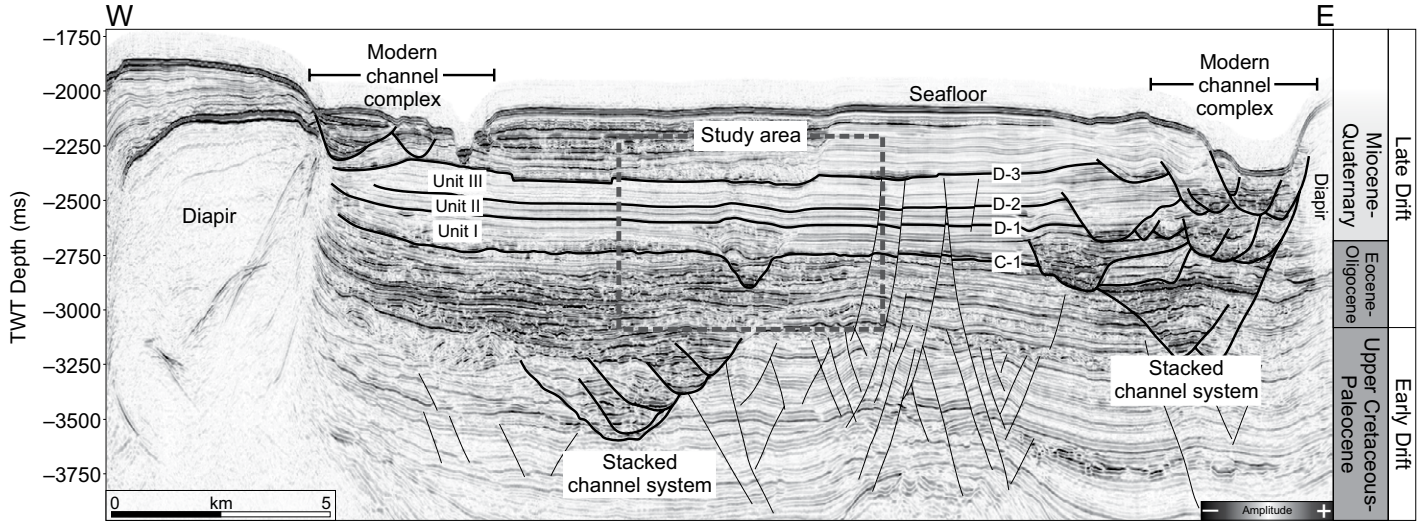

Figure 3. Seismic profile of the BES-2 survey. The study area is highlighted, and key horizons are labeled. The seismic data were correlated to the tectonic phases with a chronostratigraphic column. TWT—two-way traveltime.

was chiefly caused by differential loading of the continental margin above the Aptian salt due to sediment prograding onto the slope (Alves, 2012; Alves et al., 2009). Structural styles changed from thin-skinned extension proximal to the continental margin to diapirism in the midslope region and compression in the distal parts of the continental slope (Demercian et al., 1993; Fiduk et al., 2004; Mohriak et al., 1995; Fig. 2). Halokinesis and salt deformation in the midslope was expressed by NNW-SSE–trending salt-cored anticlines, which controlled sediment distribution within the study area (Gamboa et al., 2010).

The study area is situated above the Rio Doce Canyon system (Fiduk et al., 2004). The Rio Doce Canyon system has been evolving since the Late Cretaceous, and eight distinct episodes of canyon incision and deposition of mass-transport complexes have been identified (Alves et al., 2009; Fiduk et al., 2004). Canyon incision is believed to have been most active from the late Eocene to Oligocene, correlating with third-order lowstand systems tracts (Alves et al., 2009). Two NNW-SSE–oriented salt ridges have entrapped the Rio Doce Canyon system (Alves, 2010; Gamboa et al., 2010, 2011). These sandy turbidite fairways form potential reservoirs along the intermediate parts of the slope (Alves et al., 2009). This study focused on a single channel complex cutting through early Miocene–age pelagites, with differential compaction occurring above the channel sands (Fig. 1B).

DATA AND METHODS

The BES-2 3-D seismic survey used for this study covered an area of 1600 km^2 on the southern slope of the Abrolhos Plateau (Fig. 1A). Water depths across the study area range from 1000 to 1800 m. The data were acquired using six 5700-m-long arrays of streamers and a dual air-gun array. The seismic signal was sampled every 2 ms prior to the application of an anti-aliasing filter, giving a vertical resolution of at least 2 ms for λ/4. The calculated vertical resolution is a conservative value, as resolution reaches values of λ/8 or λ/32 in thin beds (Zeng, 2009). The data were zero-phased migrated with a bin spacing of 12.5 × 12.5 m. The processing sequence of the data included resampling, spherical divergence corrections, and zero-phase conversions undertaken prior to stacking, 3-D prestack time migration using the Stolt algorithm, and one-pass 3-D migration.

Depth was measured as two-way traveltime (TWT) in this study. No accessible wells have been drilled in the study area, so any depth conversions are based on an average velocity due to abrupt changes in lithology both vertically and horizontally around the submarine channel complex (Fig. 3).

We used a thickness-relief technique based on Perrier and Quiblier (1974), and applied in Alves and Cartwright (2010) and Alves (2012), to quantify the degree and relative timing of differential compaction over the submarine channel complex. The method uses vertical simple shear to flatten a horizon, such that the area and the vertical thickness of a horizon are preserved (Gonzalez-Mieres and Suppe, 2006).

Thickness-relief measurements follow the principle that, in a closed cross-sectional system, the area that has been displaced below a given horizon is equal to the area of relief above (Gonzalez-Mieres and Suppe, 2006). This structural method is not as easily applied to differential compaction above a channel, because the cross-sectional displacement below a given horizon does not necessarily equal the relief above it due to volume change. However, the method was changed in this work to distinguish the relative timing of differential compaction by identifying thickness changes along individual horizons (Alves, 2012; Fig. 4). Pitfalls in this method lie with inaccurate picking. Disrupted and transparent reflections (common among mass-transport complexes) lead to anomalous thickness measurements.

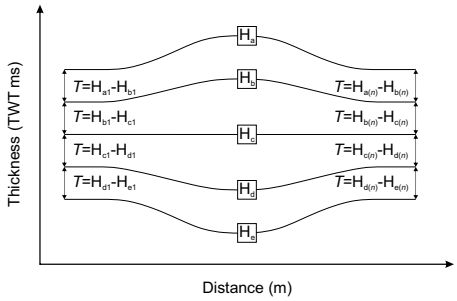

Figure 4. Summary of thickness-relief method adapted from Hubert-Ferrari et al. (2005) and Gonzalez-Mieres and Suppe (2006). It shows how the thickness was measured between two adjacent reflections. Figure is modified after Alves (2012). TWT—two-way traveltime. H—the measured horizon, assigned a letter from a-e. The subscript number refers to the point along the horizon that a measurement was taken. T—the thickness between two horizons.

In order to reduce the error from poorly picked seismic horizons, thickness measurements were compared with a mean thickness along the same horizon, such that:

$$D = T - \bar{x}_t, \quad (1)$$

where D is the difference value in TWT, T is the measured thickness, and $\bar{x}_t$ is the mean thickness along the horizon. The mean thickness was calculated using up to 791 measurements of each horizon on a cross section of the channel complex. The measurements were taken up to 1400 m either side of the channel complex axis. By subtracting the mean thickness from the measured thickness on a single horizon, a direct comparison can be made between units of different sizes. Interpretation of the graphs was aided by dividing the channel complex into three different units (Fig. 5).

Vertical thickness maps were created in Schlumberger's Petrel© to complement the analyses of differential compaction. The vertical thicknesses between successive reflections were calculated.

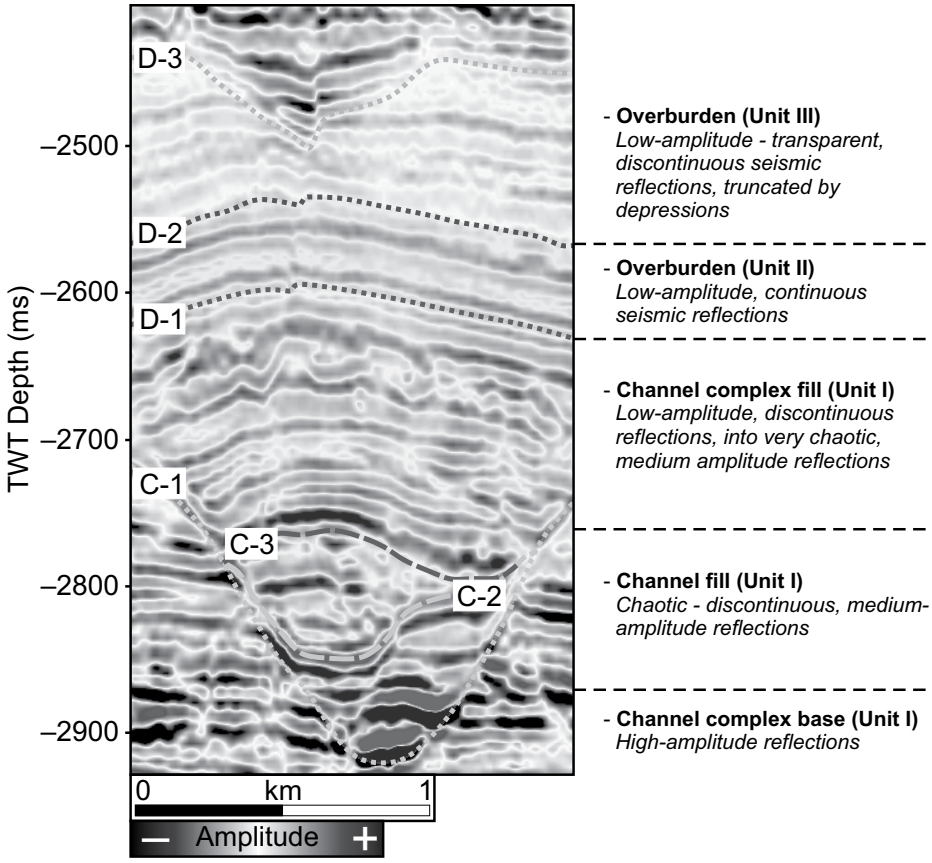

Figure 5. Summary of the different units studied. Each unit contains a description of the seismic facies, and units are bounded by the interpreted horizons. TWT—two-way traveltime.

INTERNAL CHARACTER AND GEOMETRIES OF CHANNEL AND SEAL UNITS

This study used the hierarchal classifications for submarine channels described by Abreu et al. (2003), Clark and Pickering (1996), Di Celma et al. (2011), Gardner et al. (2003), Mayall et al. (2006), and McHargue et al. (2011). Single channel-fill elements produced by incision and subsequent filling are referred to as "channels." Stacked elements of two or more channels with a similar architectural style and facies are called "channel complexes." Channels are bounded by fourth- or fifth-order surfaces, whereas a channel complex is bounded by third-order sequence boundaries (Clark and Pickering, 1996; Mayall et al., 2006). The interpreted channels have limited downslope connectivity and an irregular base (Fig. 6A).

Miocene Channel Complex

The interpreted submarine channel complex trends north to south and has an average depth of 880 ms (~800 m) below the seafloor. The maximum width of the channel complex is ~1650 m, and its maximum vertical thickness is 376 ms. Amplitude extraction between horizons C-1 and D-1 (unit I) highlights the main pathways of the channel complex (Fig. 7A). The high amplitude indicates that coarse-grained siliciclastics were deposited along its axis (McHargue et al., 2011; McHargue and Webb, 1986; Posamentier, 2003). The channel complex is filled with low-amplitude, discontinuous seismic reflections indicative of turbidite deposits (Fig. 5). Seismic reflections in the overbank units decrease in amplitude upward, indicating a transition toward more homogeneous mud deposition as the levees were buried (McHargue and Webb, 1986; Posamentier, 2003). Unit I comprises the channel complex fill described earlier herein. It is bounded at the base by horizon C-1 and at the top by horizon D-1 (Fig. 5). Henceforth, the channel complex thickness is a measure of the vertical thickness of unit I (Fig. 6A).

Channels and Knickpoints

Smaller channels are confined in the channel complex (Figs. 6A–6B). The channel thalwegs (ranging from 100 m to 400 m wide and up to 100 ms thick) follow the same path as the channel complex and occur close to the channel walls (Fig. 8B). In cross section, the channels are asymmetrical (steeper on the side closest to the channel complex margin) and do not exhibit stacking patterns (Figs. 6B and 6C). They are typically located downdip of knickpoints (Figs. 6A and 9). Channel width is smallest at the knickpoint and increases downslope, where deposition occurred (Fig. 8B). Gradients over the knickpoints reach 24°, contrasting with an average gradient along the base of the channels of <2° (Figs. 6A and 9). Immediately downslope of the knickpoints, seismic reflections are chaotic, reflecting the presence of mass-transport complexes (Alpak et al., 2013; Fig. 9). They onlap the knickpoint face and become more continuous downslope. There is a lack of connectivity and lateral continuity between these sections of channel fill; isolated pods are therefore localized in areas of greatest incision and deposition (Heiniö and Davies, 2007; Fig. 9).

Seal Units

The top of the channel-fill deposits is represented by chaotic and discontinuous seismic reflections that pinch out laterally toward the margins of the channel complex (Figs. 5 and 6B–6C). The seismic reflections are convex-up and display evidence of differential compaction above the submarine channel complex

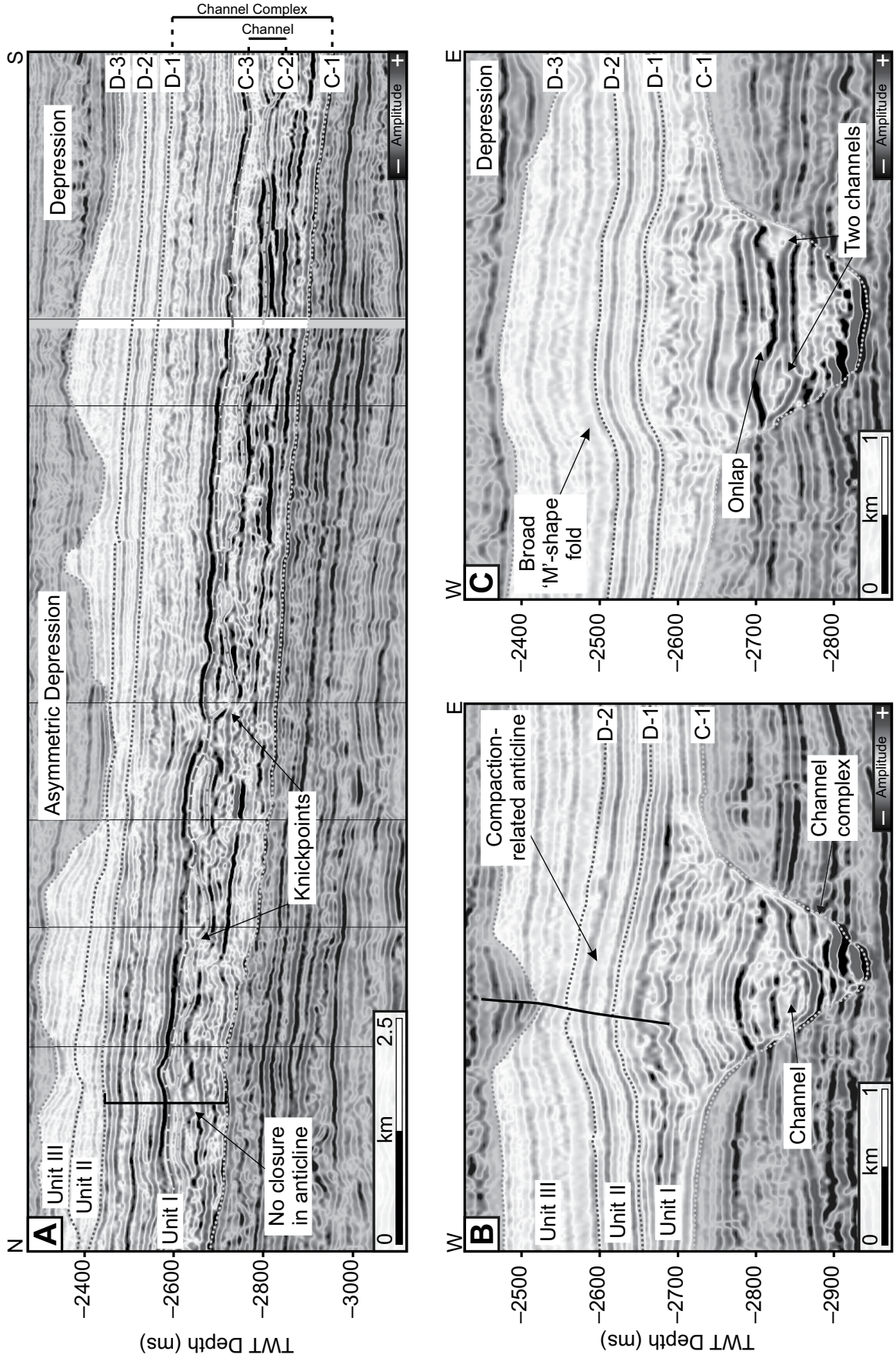

Figure 6. (A) Seismic profile along the axis of the channel complex. Knickpoints along the channels, and associated compaction, are highlighted. Asymmetric depressions are also apparent above unit III. (B) Seismic profile across the southern part of the channel. Differential compaction is very prominent here. A depression and associated fault cut through reflections above the channel complex. (C) Seismic profile through the center of the channel complex. Here, the smaller channels influence differential compaction, and a broad "M-shaped" anticline over the channel complex has formed. TWT—two-way traveltime.

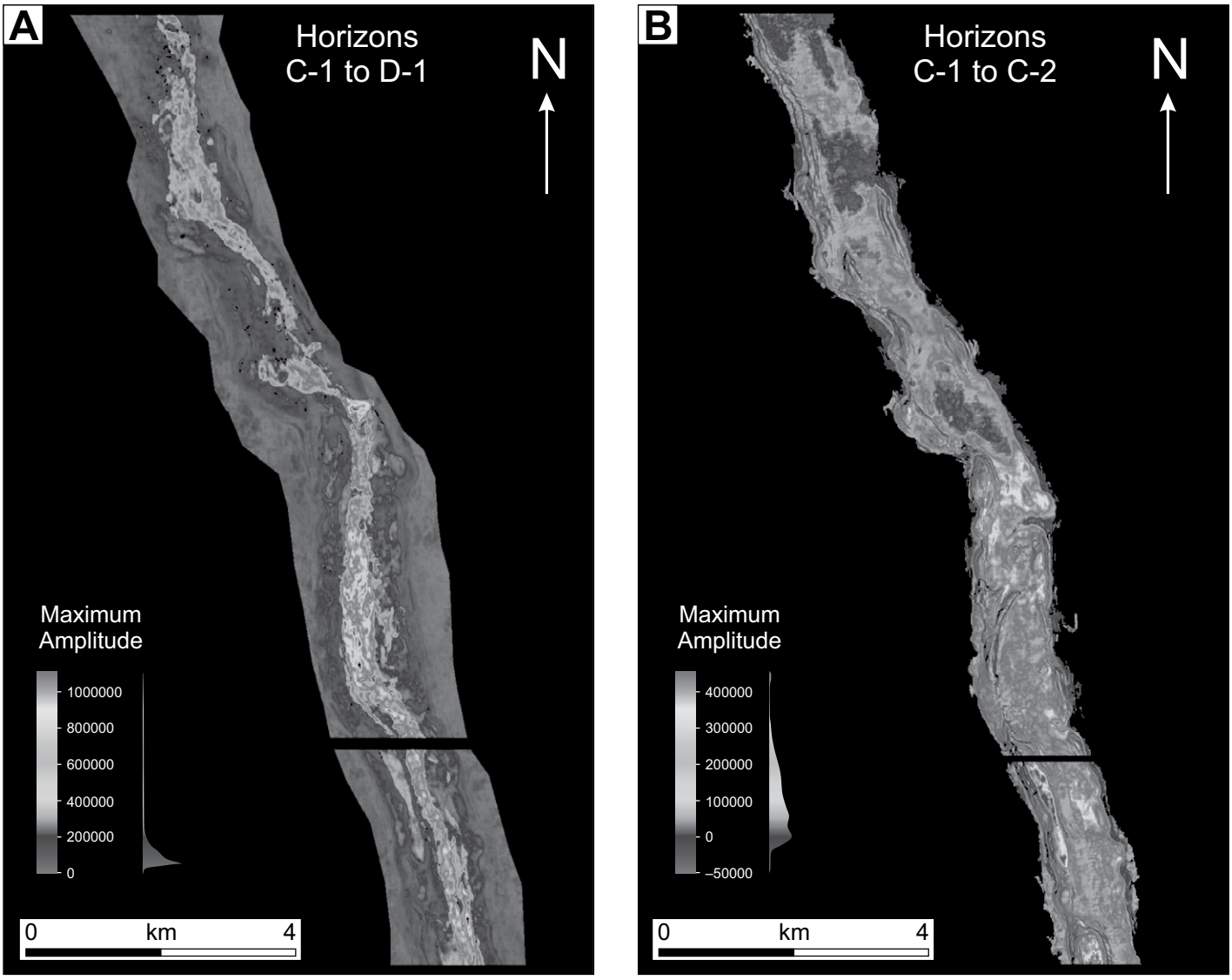

Figure 7. (A) Maximum-amplitude map of unit I (horizon C-1 to D-1). Highest-amplitude values are located on the outer bends of the channel complex. The highest-amplitude values are good indications of sand. (B) Maximum-amplitude map of the channels (C-2 to C-3). The highest amplitudes are located in the pods in the southern part of the channel complex. High-amplitude pods (as with the thickness maps) have limited continuity and are not connected.

(Figs. 6B–6C). The units above these chaotic seismic reflections are continuous and have low amplitude (Fig. 5). These low-amplitude seismic reflections are thought to represent muds deposited uniformly over the whole channel complex. There is a change to more transparent, discontinuous reflections 65 ms above the channel complex, believed to be more homogeneous muds (Fig. 5). Unit II is measured from horizon D-1 to horizon D-2 (Fig. 3). Reflections in unit II have the same amplitude, continuity, and thickness as each other. The boundary between the continuous and disrupted reflections (D-2) marks the transition from unit II to unit III.

SEISMIC GEOMETRIES RELATED TO DIFFERENTIAL COMPACTION

Convex-up structures occur within and above the studied submarine channel complex (Figs. 6B–6C). Observations made using the 3-D seismic reflection data help to explain the processes behind the formation of the anticlines and the relative timing of folding.

Compaction-Related Traps

Two magnitudes of anticlines are observed in the studied channel complex: (1) at the scale of the channel complex, forming in overburden strata (maximum height of anticline ~41 ms), and (2) at the scale of individual channels, forming downslope of knickpoints (maximum height of anticline ~29 ms; Figs. 6B–6C). The locations of the fold hinge in both examples suggest a close control of smaller channels on the loci of folding. Anticlines formed downslope of knickpoints have four-way dip closures; they onlap C-2 both upslope and downslope of the channel fill, and also the margins of the channel complex (Figs. 6B–6C and 9). Isolated "pods" delineate the path of the channels within the channel complex (Fig. 8B). The fold hinge of the larger anticline lies directly above these pods. Seismic profiles show that the occurrence of channels

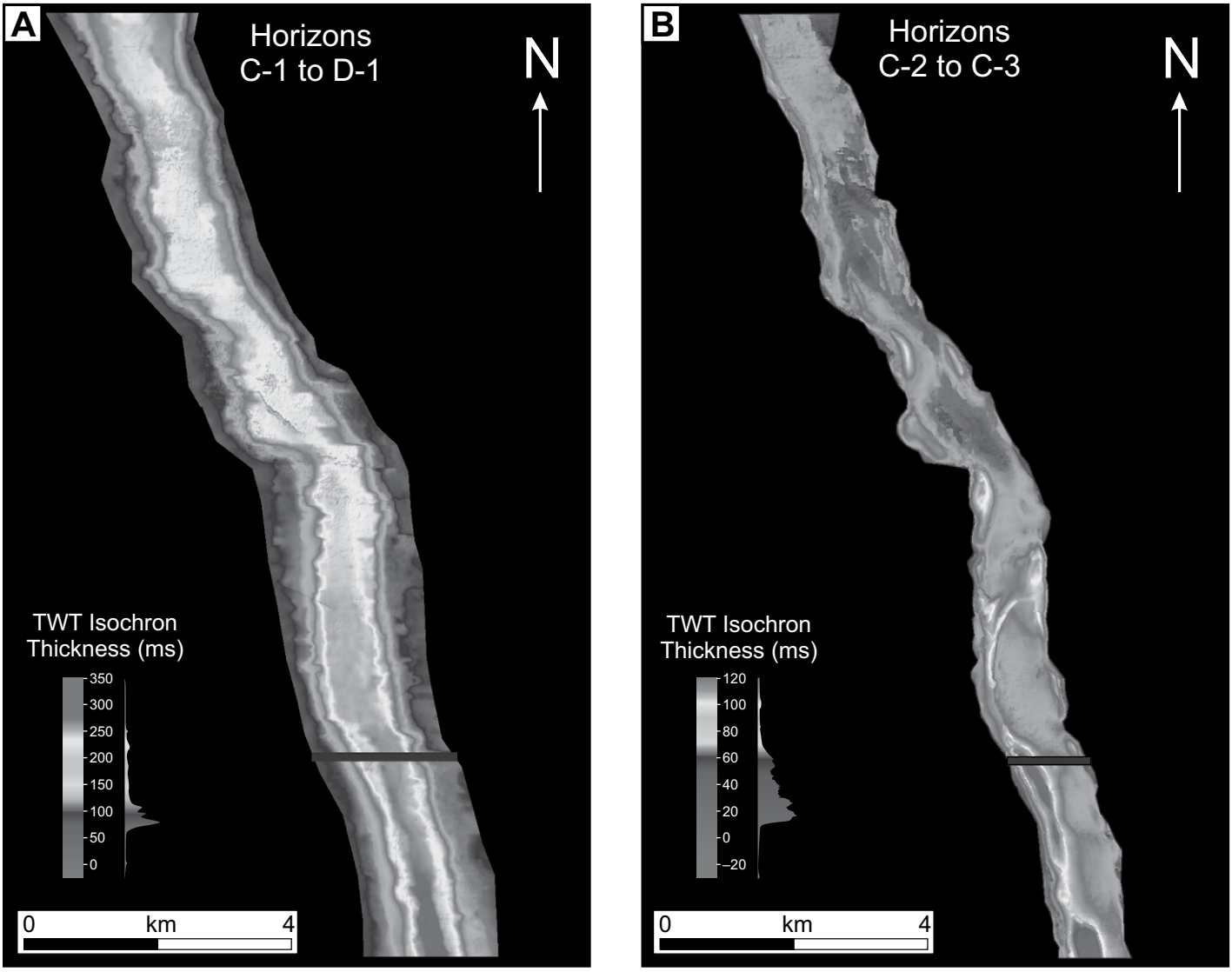

Figure 8. (A) A two-way traveltime (TWT) isochron map of the channel complex between horizons C-1 to D-1. The thickness increases downslope of the channel complex. (B) TWT isochron thickness map between horizons C-2 and C-3. Channels are easily recognizable as greatest thickness. These are downslope of knickpoints, indicating a sudden increase in the channel gradient. The thickest parts of the channels are concomitant to the widest parts of the channels.

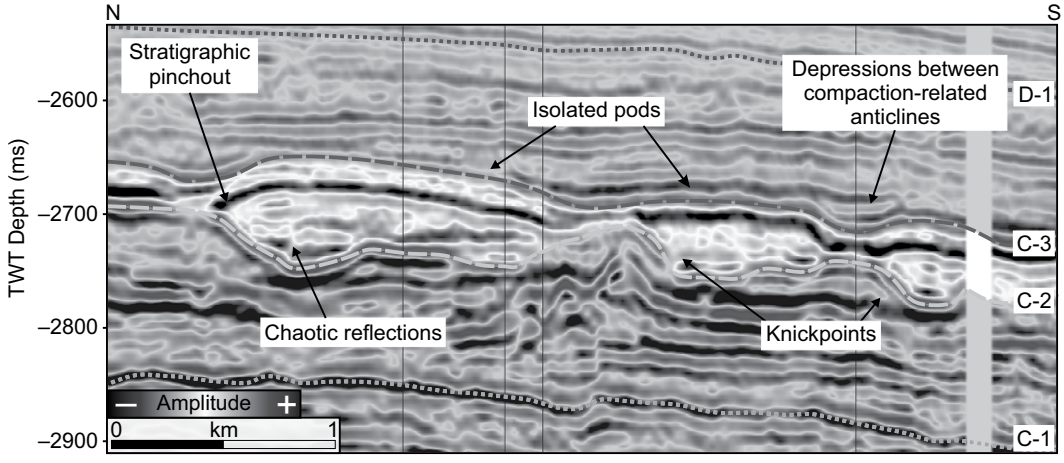

Figure 9. Seismic line running along the channel complex axis. This figure highlights the seismic facies of "pods," and the association among knickpoints, the downslope deposits, and differential compaction anticline trapping these deposits. Local depocenters form between the anticlines. TWT—two-way traveltime.

on either side of the channel complex result in a large anticline with a broad "M" shape, or a box fold (Fig. 6C), whereas a single channel, or pod, creates an anticline with a single hinge (Fig. 6A). Topographic expression of the anticline must have occurred during early burial, because reflections within unit I onlap the anticlines along horizon C-3 (Fig. 9). Accommodation space in the form of small depocenters, created by differential compaction, was later filled with sediment (Fig. 9). Seismic reflections within units II and III are continuous along the fold axis, as there is no upslope or downslope closure (Fig. 6A).

Quantification of Differential Compaction

Using the thickness-relief method, graphs were produced to compare the thicknesses of units I, II, and III (Fig. 10).

Unit 1 thickens significantly toward the axis of the channel complex (Fig. 10A). The *D* value reaches a maximum of 27 ms. Above the margins of the channel, the *D* value becomes negative, implying unit I is thinner here (Fig. 10A). This represents the boundary between more compactable mud in overbank deposits and less compactable sand in channel-fill deposits. Unit II has an equal thickness across the whole study area (~0 ms *D* value; Fig. 10B). The only change is a decrease in thickness where erosional depressions occur in unit II (Fig. 10B).

Analyses of differential compaction over unit III were only conducted in the southern part of the study area. Toward the confluence point of the two tributaries, the unit has been eroded. The unit thins on the crest of the anticline (up to 5 ms *D* value) and increases in thickness away from the channel complex, reaching a maximum *D* value of 4 ms (Fig. 10C). Therefore, differential compaction initiated at the time unit III was being deposited and produced topographic relief on the seafloor. Sediment accumulated preferentially on the flanks of the compaction-related anticline where accommodation space had increased.

STRUCTURES ASSOCIATED WITH DIFFERENTIAL COMPACTION

Differential compaction over the channel complex resulted in syn- and postdepositional structures forming in overlying strata, including anticlines, faults, and depressions. The mapped horizon in Figure 11A depicts the locations of linear and elliptical depressions running along the channel complex margins. Depressions were formed by the erosion of units II and III (Figs. 11B–11D). Elliptical and circular depressions are closely spaced in the northern part of the study area, whereas linear depressions dominate in the southern part of the study area. The long axis of each depression strikes WNW, parallel to faults below them. Widths range from ~350 to 1150 m, and lengths range from ~1725 to 4250 m. Five elliptical or linear depressions are located along the margins of the channel complex (Fig. 11A). Directly north of the central cluster of depressions is an abandoned channel tracing the east margin of the anticline, initiating north of the confluence zone and terminating in one of the central depressions (Fig. 11A).

On 3-D seismic data, the depressions have characteristic features: (1) medium- to high-amplitude, semicontinuous basal reflections; (2) a convex-downward shape, similar to the base of the channel complex (Figs. 11B–11D); (3) discontinuous, low-amplitude reflections at the top, indicative of disrupted infill (Cole et al., 2000); and (4) an asymmetric shape in cross section (Fig. 6A). Seismic reflections within the depressions normally change laterally into more continuous, lower-amplitude reflections, akin to the more homogeneous sediments deposited in units II and III (Fig. 11D).

DISCUSSION

Magnitude and Timing of Differential Compaction over Channel-Fill Deposits

Thickness-relief plots help to elucidate the timing of differential compaction. Sediment is deposited where accommodation space is created; i.e., it preferentially accumulates on the flanks of a compaction-related anticline. This is portrayed on seismic data by reflections thinning over the anticline. Small-scale variations in thickness that are lower than the resolution of the data are easier to identify with thickness-relief plots. Results show that unit II has a constant *D* value over the channel complex, whereas unit III thins on the crest of the anticline (Figs. 10B and 10C). This suggests that differential compaction over the channel complex produced a broad anticline on the seafloor between the deposition of unit II and unit III.

Because differential compaction is not uniform along the whole length of the channel complex, the variable magnitudes of differential compaction in the north and south can be explained by complex sedimentological and structural processes. We predict that differential compaction is greatest where sand is most abundant (Chopra and Marfurt, 2012; Posamentier, 2003). Figure 8A shows that the thickness of channel-fill increases toward the south. The crest of the compaction-related anticline is spatially controlled by the size and location of the less-compactable channels, which are also thicker in the south (Fig. 8B).

A process that closely controlled differential compaction in the north was the expulsion of fluids. Hence, we interpret that depressions started to form as a result of fluid expulsion at the surface. The variance map in Figure 1B shows a dense cluster of stacked depressions in the north of the study area. This suggests that the depressions formed in multiple phases; pulses of fluid expulsion during compaction are thought to have discouraged differential compaction as sands were unable to retain pore fluids. At the time fluid was putatively expelled from the channel complex, there was very little overburden. Vertical stress was low, and burial depths were not large enough to cause differential compaction.

Depressions above submarine turbidite channels have commonly been attributed to fluid expulsion and subsequent generation of pockmarks (Cole et al., 2000; Davies, 2003; Gay et al., 2003, 2006b). However, each of these studies provided evidence for fluid flow, e.g., fluid pipes or chimneys. There is no evidence for fluid migration at present in the study area, and the dimensions of the interpreted depressions are greater than the expected volume loss from the channelized reservoir. Faults connecting the channel complex with the depressions may have acted as conduits for fluid flow, but they were too small to expel enormous volumes of fluids (Bjørlykke and Høeg, 1997).

The following theory has been proposed as the process for the formation of depressions. Sand-rich turbidite channels act as a linear, secondary reservoir for fluids to drain into during compaction (Davies, 2003; Gay et al., 2003).

Figure 10 (*on following page*). Thickness-relief profiles of each unit using the differences between the measured thickness and the mean thickness between horizons, where *D* is the difference value in two-way traveltime. (A) Unit I thickness-relief profile. Maximum thickness is in the center of the channel complex, and it is thinner on the margins. (B) Unit II thickness-relief profile. There is no difference between the measured and mean thickness across the study area. (C) Unit III thickness-relief profile. The overburden has a lower measured thickness than the mean thickness over the compaction-related anticline. This indicates less deposition, and therefore topographic relief at the time of deposition.

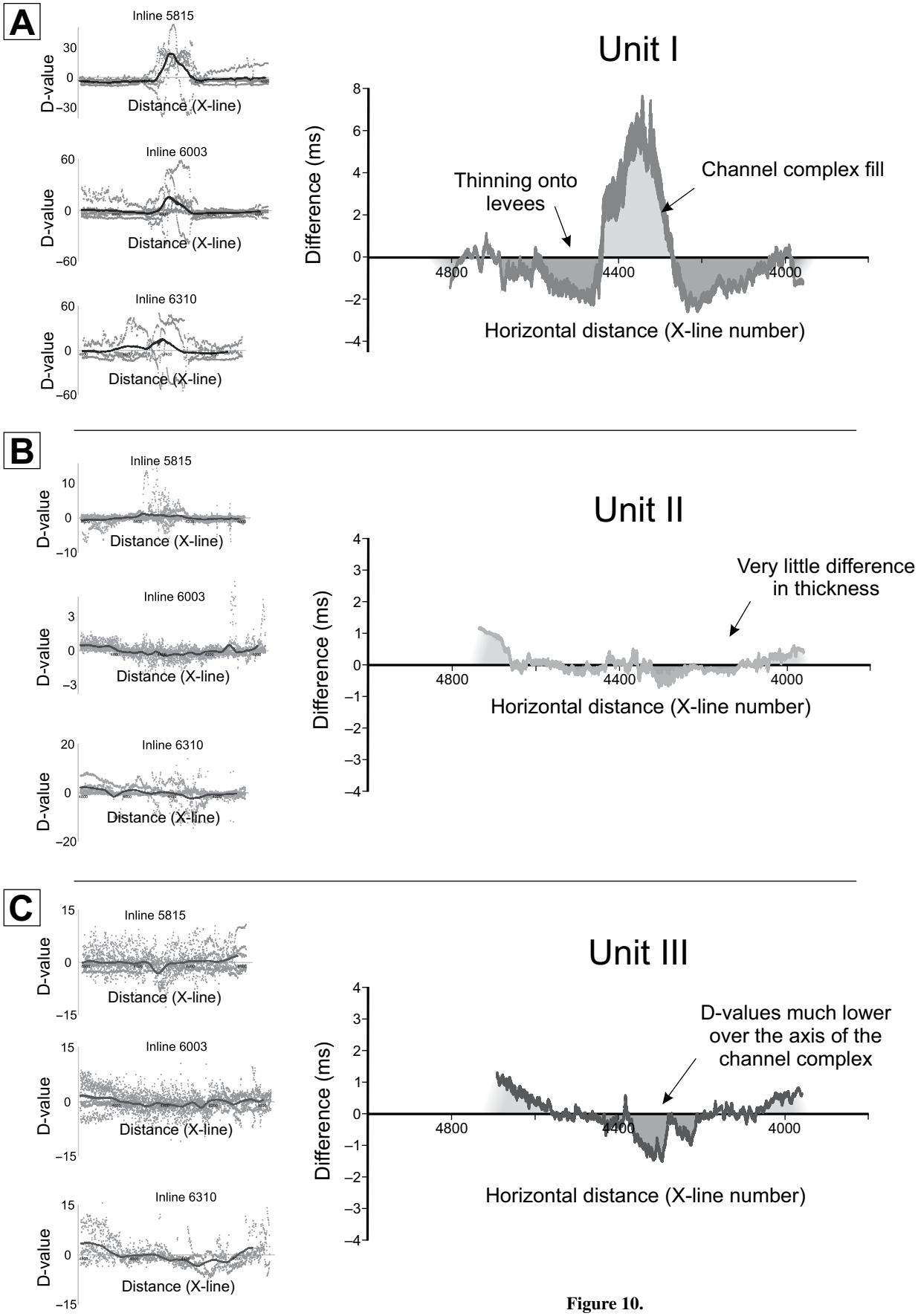
A
Inline 5815
D-value
30
0
−30
Distance (X-line)
Inline 6003
60
0
−60
Distance (X-line)
Inline 6310
60
0
−60
Distance (X-line)
Unit I
Difference (ms)
8
6
4
2
0
−2
−4
Thinning onto levees
Channel complex fill
4800
4400
4000
Horizontal distance (X-line number)
B
Inline 5815
10
0
−10
Distance (X-line)
Inline 6003
3
0
−3
Distance (X-line)
Inline 6310
20
0
−20
Distance (X-line)
Unit II
Difference (ms)
4
3
2
1
0
−1
−2
−3
−4
Very little difference in thickness
4800
4400
4000
Horizontal distance (X-line number)
C
Inline 5815
15
0
−15
Distance (X-line)
Inline 6003
15
0
−15
Distance (X-line)
Inline 6310
15
0
−15
Distance (X-line)
Unit III
Difference (ms)
4
3
2
1
0
−1
−2
−3
−4
D-values much lower over the axis of the channel complex
4800
4400
4000
Horizontal distance (X-line number)

Figure 10.

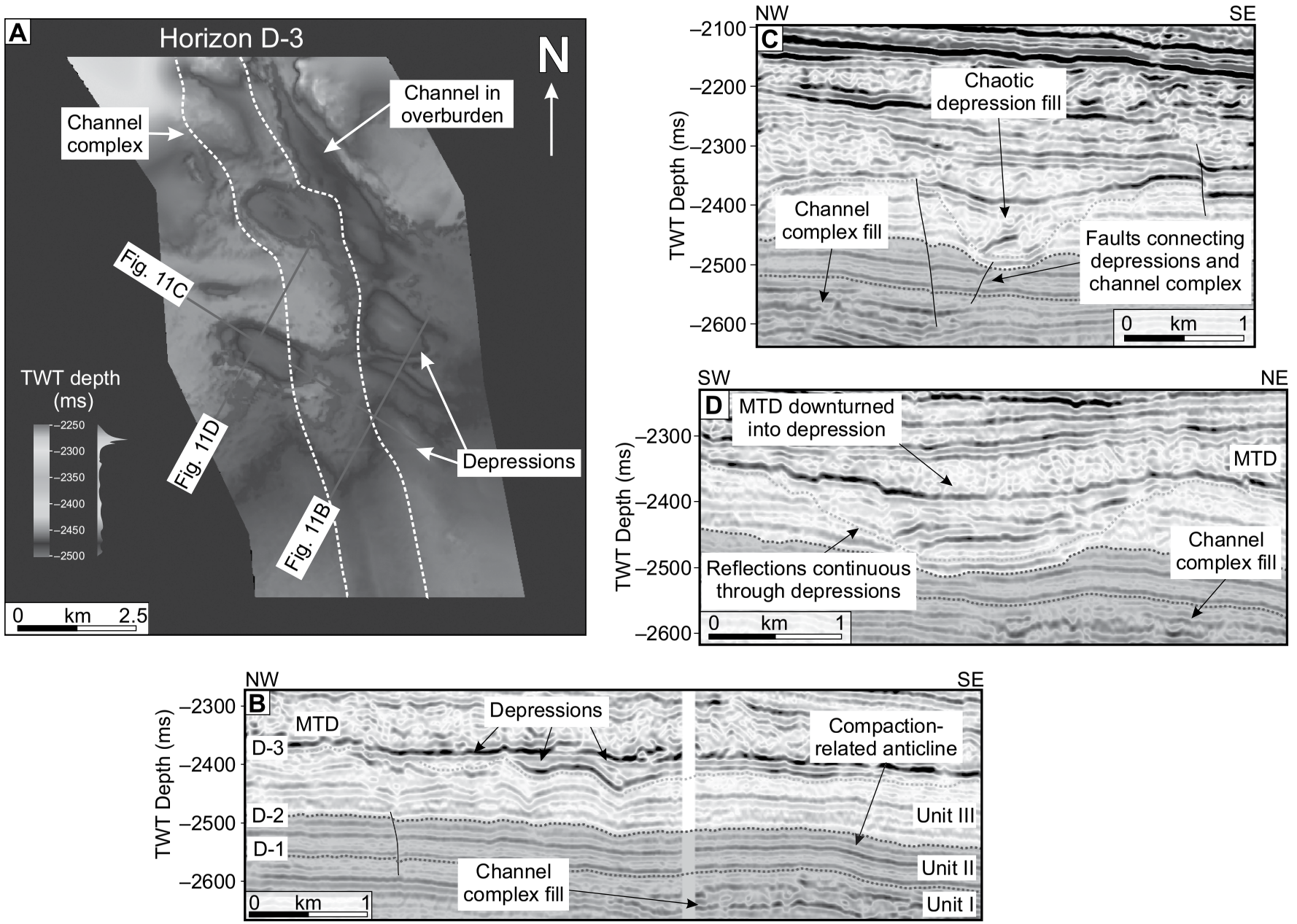

Figure 11. (A) Interpretation of horizon D-3. The channel complex below this horizon is displayed as a white line. The linear and elliptical depressions and abandoned channel. (B) Seismic profile through multiple depressions. (C) Seismic profile through the long axis of a depression. The fault connecting the depression to the channel complex is shown. The depression fill is somewhat chaotic. (D) Seismic profile through the short axis of the same depression in C. Seismic reflections above the depression are downwarped into its center. Reflections bounding the depressions continue through it with a lower amplitude. TWT—two-way traveltime; MTD—mass-transport deposit.

Rapid sedimentation and loading in the study area (>100 m m.y.$^{-1}$) cause channel sands to become overpressured, a process enhanced by differential compaction of the sands and lateral overbank muds (Gay et al., 2003, 2006a). Rapidly deposited muds overlying the channel complex had low mechanical strength, and small increases in pore pressure within the underlying sands were sufficient to fracture the rock and allow migration of fluids to the surface (Carver, 1968; Davies, 2003; Gay et al., 2006a). Fluid migration occurred if overpressure in the channel fill was greater than the maximum horizontal stress and if the vertical stress was relatively low (Bjørlykke and Høeg, 1997). This would have formed pockmarks on the seafloor where sediment had become fluidized. The line of depressions seen on the structural map in Figure 11A is parallel with the buried channel complex and corresponding compaction-related anticline. The depressions strike perpendicular to the predicted deep-water paleocurrents along the Brazilian margin (Duarte and Viana, 2007). Therefore, localized erosion where pockmarks formed could have led to the large depressions seen in the seismic data (Viana, 2001). Figure 12 is a cartoon summarizing the proposed mechanisms for trap formation, faulting and fluid expulsion, and the bottom current erosion of pockmarks.

Differential Compaction as a Process Leading to Trap Formation over Submarine Channels

Coarse-grained channel turbidites in deep-water settings are common exploration targets in southeast Brazil (Clark and Pickering, 1996; Gamboa and Alves, 2015; Mayall et al., 2006; Viana et al., 2003). Turbidite sands along channel axes have high porosity and permeability, permitting the migration of hydrocarbons (Clark and Pickering, 1996). Muds and shales draping the channel fill and deposited within the channel complex may provide significant stratigraphic traps, though this heterogeneity in lithology can lead to major risks to exploration and recovery of hydrocarbons (Gamboa and Alves, 2015; Mayall et al., 2006; McHargue and Webb, 1986). Amplitude maps are a good indication for the location of channel sands. Figure 7 shows high amplitudes along the axis of the channel complex. There is continuity of the high amplitude along slope, indicating a possible pathway for migration of hydrocarbons. Within many submarine turbidite systems, channels are stacked vertically and horizontally. This dramatically increases reservoir connectivity, ensuring that fluids migrate over long distances along multiple channel axes. The studied channel complex, however, is isolated

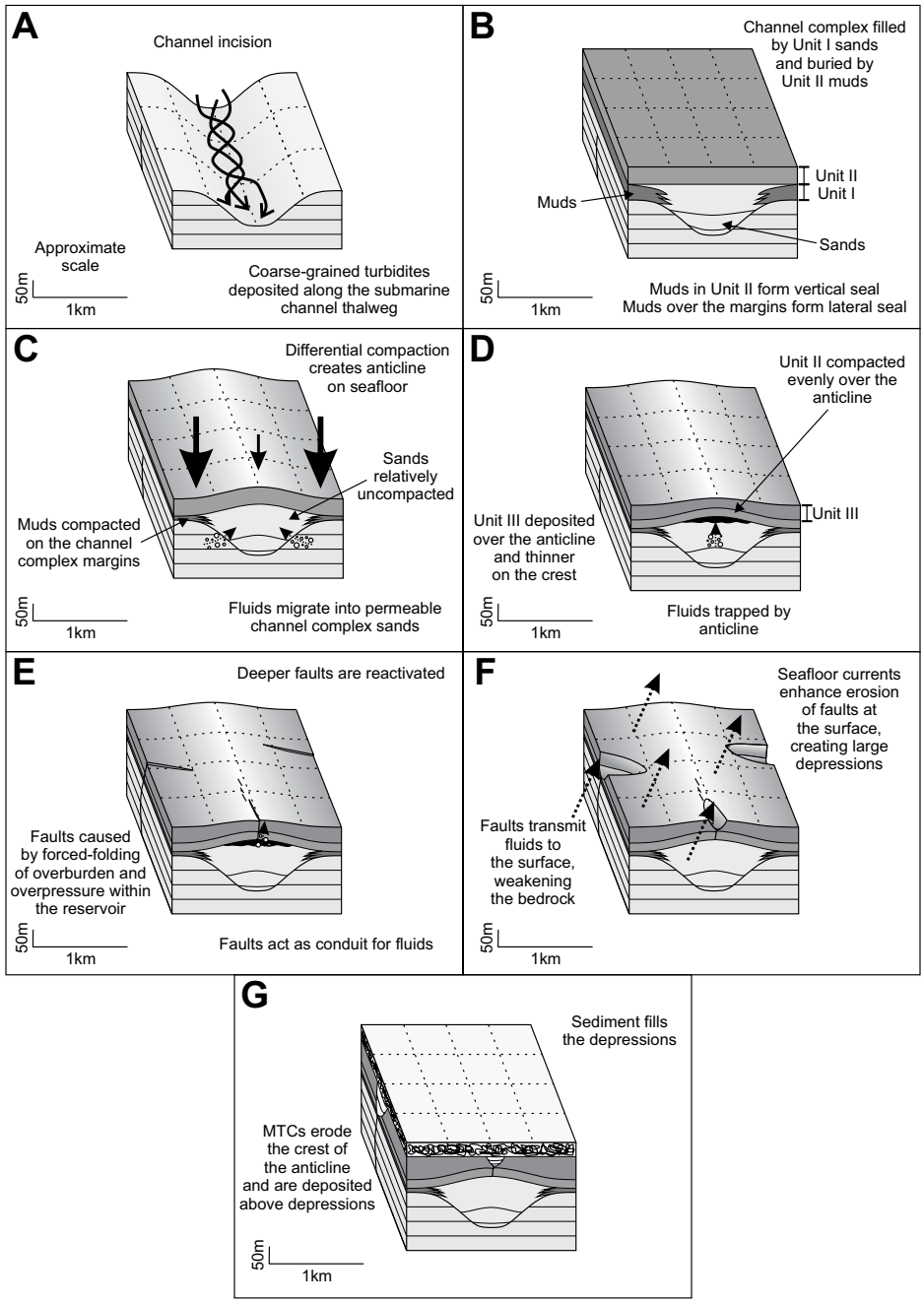

Figure 12. Cartoon showing the evolution of differential compaction, deposition of units I, II, and III, migration of fluids, and the formation of faults/depressions. (A) Seafloor is incised by turbidity flows. (B) Channel complex is filled with unit I sands and muds and then overlain with unit II muds. (C) Differential compaction starts, and the channel complex margins compact more than channel-fill sands. Fluids subsequently migrate into the sand reservoir. (D) Unit III muds are deposited over the positive-relief seafloor structure. (E) Overpressure in the reservoir leads to faults forming in the overburden, transmitting fluids to the surface. (F) Fluids weaken the rocks at the fault tips and forms depressions that are enhanced by erosion due to seafloor currents. (G) Sediment fills the depressions, and mass-transport deposits erode and bury unit III. MTC—mass-transport complex.

and shows no evidence of channel migration or aggradation. Another caveat is the lack of upslope dip-closure of the compaction-related anticline (Fig. 6A). The observed E-W closure of the anticline over the flanks of the channel complex provides a suitable lateral trap, but hydrocarbons are likely to travel upslope, where no evidence of trap closure is seen on the northern limit of the seismic data.

Deposition of coarse sediment downslope of knickpoints enhances reservoir quality. The sudden decrease in gradient at the base of the knickpoints reduces flow velocity, so entrained coarse sediment and mass-transport complexes are deposited (Alpak et al., 2013). Chaotic seismic reflections representing slumps and debrites onlap and pinch out onto the muddy slope draping over the knickpoints (Prather, 2003). The muds act as a permeability barrier and form an updip stratigraphic trap. Differential compaction over the deposits downslope of the knickpoints creates anticlines with four-way dip closure. However, limited flow communication between the "pods" compartmentalizes these reservoirs. Because the migration of hydrocarbons between isolated pods relies on a carrier bed, e.g., basal sands along the channel complex (Schowalter, 1979), this scenario can lead to "fill-to-spill" traps, where hydrocarbons fill a single pod or reservoir until it reaches a spill point. The hydrocarbons travel upslope, along a permeable bed, and fill the next pod. This is the most likely model for charging similar reservoirs to the study areas downslope of channel knickpoints.

In this study, we estimated the magnitudes of differential compaction in the time domain. In order to assess and understand the results and interpretations presented, the limitations of not converting the data into depth in meters needs to be considered. As there are no accessible wells drilled into the studied channel, the small-scale changes in lithology, and therefore seismic velocity, are unknown. Seismic velocity through consolidated sands is greater than in shales and muds (Farmer and Jumikis, 1968). Taking this into account, we expect the compaction-related anticline to be larger than that measured on the TWT seismic data used in this paper.

CONCLUSIONS

This study used thickness-relief plots and seismic volume attributes to help understand how and when differential compaction occurred over a submarine channel complex in the Espírito Santo Basin, Brazil. Our results show the following features:

(1) Differential compaction over the channel complex occurred during early burial. Results from the thickness-relief method indicate the compaction-related anticline was expressed on the surface after the channel was buried by ~200 m of sediment. The anticline reached a maximum magnitude of 41 ms (~37 m) in the south.

(2) Fluid expulsion limited differential compaction over the channel complex. Elliptical and linear depressions are observed on seismic data. Fluids from within the channel sands were transmitted to the seafloor by a set of faults on the channel complex margin. Deep-water paleocurrents over the buried channel removed fluidized sediment and eroded the depressions. Subsequent scouring and collapse of the steep walls rapidly increased their size. There are more depressions in the north of the channel complex, where differential compaction is not as prominent, due to the expulsion of larger volumes of fluid from the channel complex compared with the south.

(3) Knickpoints on submarine channels within the channel complex are associated with "pods" of coarse-grained deposits, including slumps, slides, and debris flows. There are limited connectivity and lateral continuity of the pods. Differential compaction over the units downslope of knickpoints isolated the pods.

(4) Possible reservoir rocks are identified along the base of the channel complex and in pods downslope of knickpoints. The compaction-related anticline above the channel complex has no upslope closure; the trapping potential is limited. However, the isolated pods onlap the knickpoint faces, indicating stratigraphic trapping potential, and they have four-way dip closure above them.

(5) The identified petroleum system relies on hydrocarbon migration along the base of the channel complex. We propose a fill-to-spill model for charging these reservoirs, where the hydrocarbons migrated into a pod, and when the spill point was reached, they migrated updip into the next pod along the channel complex.

(6) These findings suggest that suitable structural and stratigraphic traps form during early burial of a submarine channel. Analogues can be made to submarine channels in similar basins on passive margins such as the Gulf of Mexico and the west coast of Africa.

ACKNOWLEDGMENTS

The work contained in this paper was conducted during a Ph.D. study undertaken as part of the Natural Environment Research Council (NERC) Centre for Doctoral Training (CDT) in Oil and Gas and was funded by NERC and cosponsored by Cardiff University, whose support is gratefully acknowledged. CGG© is acknowledged for the provision of data for this research paper. We acknowledge Schlumberger (Petrel©) for granting provisions of academic licenses to Cardiff's 3-D Seismic Laboratory. We thank the reviewers, I. Davison, T. Wrona, and J. Ochoa, for their suggestions and improvements to the initial manuscript, and D. Schofield for editorial support.

REFERENCES CITED

Abreu, V., Sullivan, M., Pirmez, C., and Mohrig, D., 2003, Lateral accretion packages (LAPs): An important reservoir element in deep water sinuous channels: Marine and Petroleum Geology, v. 20, no. 6-8, p. 631–648, doi: 10.1016/j.marpetgeo.2003.08.003.

Alpak, F.O., Barton, M.D., and Naruk, S.J., 2013, The impact of fine-scale turbidite channel architecture on deep-water reservoir performance: American Association of Petroleum Geology Bulletin, v. 97, no. 2, p. 251–284, doi:10.1306/04021211067.

Alves, T.M., 2010, 3D seismic examples of differential compaction in mass-transport deposits and their effect on post-failure strata: Marine Geology, v. 271, no. 3-4, p. 212–224, doi:10.1016/j.margeo.2010.02.014.

Alves, T.M., 2012, Scale-relationships and geometry of normal faults reactivated during gravitational gliding of Albian rafts (Espírito Santo Basin, SE Brazil): Earth and Planetary Science Letters, v. 331-332, p. 80–96, doi:10.1016/j.epsl.2012.03.014.

Alves, T.M., and Cartwright, J.A., 2010, The effect of mass-transport deposits on the younger slope morphology, offshore Brazil: Marine and Petroleum Geology, v. 27, no. 9, p. 2027–2036, doi:10.1016/j.marpetgeo.2010.05.006.

Alves, T.M., Cartwright, J., and Davies, R.J., 2009, Faulting of salt-withdrawal basins during early halokinesis: Effects on the Paleogene Rio Doce Canyon system (Espírito Santo Basin, Brazil): American Association of Petroleum Geology Bulletin, v. 93, no. 5, p. 617–652, doi:10.1306/02030908105.

Athy, L.F., 1930, Density, porosity, and compaction of sedimentary rocks: American Association of Petroleum Geology Bulletin, v. 14, no. 1, p. 1–24.

Baudon, C., and Cartwright, J., 2008, The kinematics of reactivation of normal faults using high resolution throw mapping: Journal of Structural Geology, v. 30, p. 1072–1084, doi:10.1016/j.jsg.2008.04.008.

Bjørlykke, K., and Høeg, K., 1997, Effects of burial diagenesis on stresses, compaction and fluid flow in sedimentary basins: Marine and Petroleum Geology, v. 14, no. 3, p. 267–276, doi:10.1016/S0264-8172(96)00051-7.

Carver, R.E., 1968, Differential compaction as a cause of regional contemporaneous faults: American Association of Petroleum Geology Bulletin, v. 52, no. 3, p. 414–419.

Chang, H.K., Kowsmann, R.O., Figueiredo, A.M.F., and Bender, A., 1992, Tectonics and stratigraphy of the East Brazil Rift system: An overview: Tectonophysics, v. 213, no. 1-2, p. 97–138, doi:10.1016/0040-1951(92)90253-3.

Chopra, S., and Marfurt, K.J., 2012, Seismic attribute expression of differential compaction: The Leading Edge, v. 31, no. 12, p. 1418–1422, doi:10.1190/tle31121418.1.

Clark, J.D., and Pickering, K.T., 1996, Architectural elements and growth patterns of submarine channels: Application to hydrocarbon exploration: American Association of Petroleum Geology Bulletin, v. 80, no. 2, p. 194–220.

Cole, D., Stewart, S., and Cartwright, J., 2000, Giant irregular pockmark craters in the Palaeogene of the outer Moray Firth basin, UK North Sea: Marine and Petroleum Geology, v. 17, no. 5, p. 563–577, doi:10.1016/S0264-8172(00)00013-1.

Corcoran, J., 2006, Application of a sealing surface classification for stratigraphic related traps in the UK Central North Sea, *in* Allen, M.R., Goffey, G.P., Morgan, R.K., and Walker, I.M., eds., The Deliberate Search for the Stratigraphic Trap: Geological Society, London, Special Publication 254, p. 207–223, doi:10.1144/GSL.SP.2006.254.01.11.

Cosgrove, J.W., and Hillier, R.D., 1999, Forced-fold development within Tertiary sediments of the Alba Field, UKCS: Evidence of differential compaction and post-depositional sandstone remobilization, *in* Cosgrove, J.W., and Ameen, M.S., eds., Forced Folds and Fractures: Geological Society, London, Special Publication 169, p. 61–71, doi:10.1144/GSL.SP.2000.169.01.05.

Davies, R.J., 2003, Kilometer-scale fluidization structures formed during early burial of a deep-water slope channel on the Niger Delta: Geology, v. 31, no. 11, p. 949–952, doi:10.1130/G19835.1.

Davison, I., 1999, Tectonics and hydrocarbon distribution along the Brazilian South Atlantic margin, *in* Cameron, N.R., Bate, R.H., and Clure, V.S., eds., The Oil and Gas Habitats of the South Atlantic: Geological Society, London, Special Publication 153, p. 133–151, doi:10.1144/GSL.SP.1999.153.01.09.

Demercian, S., Szatmari, P., and Cobbold, P., 1993, Style and pattern of salt diapirs due to thin-skinned gravitational gliding, Campos and Santos Basins, offshore Brazil: Tectonophysics, v. 228, no. 3-4, p. 393–433, doi:10.1016/0040-1951(93)90351-J.

Di Celma, C.N., Brunt, R.L., Hodgson, D.M., Flint, S.S., and Kavanagh, J.P., 2011, Spatial and temporal evolution of a Permian submarine slope channel–levee system, Karoo Basin, South Africa: Journal of Sedimentary Research, v. 81, no. 8, p. 579–599, doi:10.2110/jsr.2011.49.

Duarte, C.S., and Viana, A.R., 2007, Santos Drift system: Stratigraphic organization and implications for late Cenozoic palaeocirculation in the Santos Basin, SW Atlantic Ocean, *in* Viana, A.R., and Rebesco, M., eds., Economic and Palaeoceanographic Significance of Contourite Deposits: Geological Society, London, Special Publication 276, p. 171–198, doi:10.1144/GSL.SP.2007.276.01.09.

Farmer, I.W., and Jumikis, A.R., 1968, Engineering Properties of Rocks: London, Spon Limited, 180 p.

Fiduk, J.C., Brush, E.R., Anderson, L.E., Gibbs, P.B., and Rowan, M.G., 2004, Salt deformation, magmatism, and hydrocarbon prospectivity in the Espirito Santo Basin, offshore Brazil, *in* Post, P.J., Olson, D.L., Lyons, K.T., Palmes, S.L., Harison, P.F., Rosen, N.C., eds., Proceedings Salt-Sediment Interactions and Hydrocarbon Prospectivity: Concepts, Applications, and Case Studies for the 21st Century: Proceedings of Gulf Coast Section SEPM Foundation Bob F. Perkins Research Conference 2004: Society for Sedimentary Geology (SEPM), p. 370–392.

Gamboa, D., and Alves, T.M., 2015, Spatial and dimensional relationships of submarine slope architectural elements: A seismic-scale analysis from the Espírito Santo Basin (SE Brazil): Marine and Petroleum Geology, v. 64, p. 43–57, doi:10.1016/j.marpetgeo.2015.02.035.

Gamboa, D., Alves, T., Cartwright, J., and Terrinha, P., 2010, MTD distribution on a 'passive' continental margin: The Espírito Santo Basin (SE Brazil) during the Palaeogene: Marine and Petroleum Geology, v. 27, no. 7, p. 1311–1324, doi:10.1016/j.marpetgeo.2010.05.008.

Gamboa, D., Alves, T., and Cartwright, J., 2011, Distribution and characterization of failed (mega) blocks along salt ridges, southeast Brazil: Implications for vertical fluid flow on continental margins: Journal of Geophysical Research–Solid Earth (1978–2012), v. 116, no. B8, B08103, doi:10.1029/2011JB008357.

Gardner, M.H., Borer, J.M., Melick, J.J., Mavilla, N., Dechesne, M., and Wagerle, R.N., 2003, Stratigraphic process-response model for submarine channels and related features from studies of Permian Brushy Canyon outcrops, west Texas: Marine and Petroleum Geology, v. 20, no. 6-8, p. 757–787, doi:10.1016/j.marpetgeo.2003.07.004.

Gay, A., Lopez, M., Cochonat, P., Sultan, N., Cauquil, E., and Brigaud, F., 2003, Sinuous pockmark belt as indicator of a shallow buried turbiditic channel on the lower slope of the Congo Basin, West African margin, *in* Van Rensbergen, P., Hillis, R.R., Maltman, A.J., and Morley, C.K., eds., Subsurface Sediment Mobilization: Geological Society, London, Special Publication 216, p. 173–189, doi:10.1144/GSL.SP.2003.216.01.12.

Gay, A., Lopez, M., Cochonat, P., Levaché, D., Sermondadaz, G., and Seranne, M., 2006a, Evidences of early to late fluid migration from an Upper Miocene turbiditic channel revealed by 3D seismic coupled to geochemical sampling within seafloor pockmarks, Lower Congo Basin: Marine and Petroleum Geology, v. 23, no. 3, p. 387–399, doi:10.1016/j.marpetgeo.2006.02.004.

Gay, A., Lopez, M., Cochonat, P., Séranne, M., Levaché, D., and Sermondadaz, G., 2006b, Isolated seafloor pockmarks linked to BSRs, fluid chimneys, polygonal faults and stacked Oligocene–Miocene turbiditic palaeochannels in the Lower Congo Basin: Marine Geology, v. 226, no. 1-2, p. 25–40, doi:10.1016/j.margeo.2005.09.018.

Gonzalez-Mieres, R., and Suppe, J., 2006, Relief and shortening in detachment folds: Journal of Structural Geology, v. 28, no. 10, p. 1785–1807, doi:10.1016/j.jsg.2006.07.001.

Heiniö, P., and Davies, R.J., 2007, Knickpoint migration in submarine channels in response to fold growth, western Niger Delta: Marine and Petroleum Geology, v. 24, no. 6-9, p. 434–449, doi:10.1016/j.marpetgeo.2006.09.002.

Heritier, F., Lossel, P., and Wathne, E., 1980, Frigg Field—Large submarine-fan trap in Lower Eocene rocks of the Viking graben, North Sea, *in* Halbouty, M.T., ed., Giant Oil and Gas Fields of the Decade 1968–1978: American Association of Petroleum Geologists Bulletin, v. 30, p. 59–79.

Howard, A.D., Dietrich, W.E., and Seidl, M.A., 1994, Modeling fluvial erosion on regional to continental scales: Journal of Geophysical Research–Solid Earth, v. 99, no. B7, p. 13,971–13,986, doi:10.1029/94JB00744.

Hubert-Ferrari, A., Suppe, J., Wang, X. and Jia, C., 2005, Yakeng detachment fold, South Tianshan, China, in Seismic Interpretation of Contractional Fault-related Folds: American Association of Petroleum Geologists Seismic Atlas, p. 110–113.

Mayall, M., Jones, E., and Casey, M., 2006, Turbidite channel reservoirs—Key elements in facies prediction and effective development: Marine and Petroleum Geology, v. 23, no. 8, p. 821–841, doi:10.1016/j.marpetgeo.2006.08.001.

McHargue, T.R., and Webb, J.E., 1986, Internal geometry, seismic facies, and petroleum potential of canyons and inner fan channels of the Indus submarine fan: American Association of Petroleum Geology Bulletin, v. 70, no. 2, p. 161–180.

McHargue, T., Pyrcz, M.J., Sullivan, M.D., Clark, J., Fildani, A., Romans, B., Covault, J., Levy, M., Posamentier, H., and Drinkwater, N., 2011, Architecture of turbidite channel systems on the continental slope: Patterns and predictions: Marine and Petroleum Geology, v. 28, no. 3, p. 728–743, doi:10.1016/j.marpetgeo.2010.07.008.

Mohriak, W.U., Rabelo, J.L., De Matos, R.D., and De Barros, M.C., 1995, Deep seismic reflection profiling of sedimentary basins offshore Brazil: Geological objectives and preliminary results in the Sergipe Basin: Journal of Geodynamics, v. 20, no. 4, p. 515–539, doi:10.1016/0264-3707(95)00024-4.

Mohriak, W.U., Nemčok, M., and Enciso, G., 2008, South Atlantic divergent margin evolution: Rift-border uplift and salt tectonics in the basins of SE Brazil, *in* Pankhurst, R.J., Trouw, R.A.J., de Brito Neves, B.B., and de Wit, M.J., eds., West Gondwana: Pre-Cenozoic Correlations Across the South Atlantic Region: Geological Society, London, Special Publication 294, p. 365–398, doi:10.1144/SP294.19.

Ojeda, H., 1982, Structural framework, stratigraphy, and evolution of Brazilian marginal basins: American Association of Petroleum Geology Bulletin, v. 66, no. 6, p. 732–749.

Osborne, M.J., and Swarbrick, R.E., 1997, Mechanisms for generating overpressure in sedimentary basins: A reevaluation: American Association of Petroleum Geology Bulletin, v. 81, no. 6, p. 1023–1041.

Perrier, R., and Quiblier, J., 1974, Thickness changes in sedimentary layers during compaction history; methods for quantitative evaluation: American Association of Petroleum Geology Bulletin, v. 58, no. 3, p. 507–520.

Posamentier, H.W., 2003, Depositional elements associated with a basin floor channel-levee system: Case study from the Gulf of Mexico: Marine and Petroleum Geology, v. 20, no. 6-8, p. 677–690, doi:10.1016/j.marpetgeo.2003.01.002.

Prather, B.E., 2003, Controls on reservoir distribution, architecture and stratigraphic trapping in slope settings: Marine and Petroleum Geology, v. 20, no. 6-8, p. 529–545, doi:10.1016/j.marpetgeo.2003.03.009.

Schowalter, T.T., 1979, Mechanics of secondary hydrocarbon migration and entrapment: American Association of Petroleum Geology Bulletin, v. 63, no. 5, p. 723–760.

Trask, P.D., 1931, Compaction of sediments: American Association of Petroleum Geology Bulletin, v. 15, no. 3, p. 271–276.

Viana, A.R., 2001, Seismic expression of shallow-to deep-water contourites along the south-eastern Brazilian margin: Marine Geophysical Researches, v. 22, no. 5-6, p. 509–521, doi:10.1023/A:1016307918182.

Viana, A.R., Figueiredo, A., Faugres, J.-C., Lima, A., Gonthier, E., Brehme, I., and Zaragosi, S., 2003, The Sao Tom deep-sea turbidite system (southern Brazil Basin): Cenozoic seismic stratigraphy and sedimentary processes: American Association of Petroleum Geology Bulletin, v. 87, no. 5, p. 873–894, doi:10.1306/12100201048.

Wood, J.M., and Hopkins, J.C., 1989, Reservoir sandstone bodies in estuarine valley fill: Lower Cretaceous Glauconitic Member, Little Bow Field, Alberta, Canada: American Association of Petroleum Geology Bulletin, v. 73, no. 11, p. 1361–1382.

Wood, J.M., and Hopkins, J.C., 1992, Traps associated with paleovalleys and interfluves in an unconformity bounded sequence: Lower Cretaceous Glauconitic Member, southern Alberta, Canada (1): American Association of Petroleum Geology Bulletin, v. 76, no. 6, p. 904–926.

Xu, S., Hao, F., Xu, C., Wang, Y., Zou, H., and Gong, C., 2015, Differential compaction faults and their implications for fluid expulsion in the northern Bozhong subbasin, Bohai Bay Basin, China: Marine and Petroleum Geology, v. 63, p. 1–16, doi:10.1016/j.marpetgeo.2015.02.013.

Zeng, H., 2009, How thin is a thin bed? An alternative perspective: The Leading Edge, v. 28, no. 10, p. 1192–1197, doi:10.1190/1.3249773.

Science Editor: David I. Schofield
Associate Editor: Peter Eichhubl

Manuscript Received 19 September 2016
Revised Manuscript Received 6 June 2017
Manuscript Accepted 11 July 2017

Printed in the USA